MNC-4028-0021

ANNUAL PROGRESS REPORT

"RESEARCH IN NUCLEAR CHEMISTRY"

Department of Chemistry
University of Maryland
College Park, Maryland 20742

Professor V. E. Viola, Jr.
Professor G. E. Gordon
Professor W. B. Walters

November 1, 1974

This work supported in part by the U.S. Atomic Energy Commission under contract AT(40-1)-4028

TABLE OF CONTENTS

G. Decay of ^{195}Os and Search for ^{196}Os

In conjunction with our investigation of (p,3pxn) reaction systematics (see Sect. 7.1.1), we have initiated a program to study the very neutron-rich ^{195}Os and ^{196}Os isotopes. At present, ^{196}Os is clearly still undiscovered, while the assignment and characterization of ^{195}Os is questionable. Rey and Baro [G. Baro and P. Rey, Z. Naturforschung 12A (1957) 520 abstract only; P. Rey and G. B. Baro, Publs. Com. Nacl. Energia Atomica Republica Argentina 1 (1957) 115] on irradiation of platinum with fast neutrons observed and assigned a 6.5-min activity to ^{195}Os. These authors using a Feather analysis obtained a maximum β-energy of 2 MeV, and observed a genetic relationship with the then-known ^{195}Ir daughter. Unfortunately, the then-existing assignment for ^{195}Ir has subsequently been identified as ^{81}Rb, arising from reactions induced in target impurities [K. J. Hofstetter and P. J. Daly, Nucl. Phys. A106 (1968) 382]. As a result, the present assignment of ^{195}Os will not withstand careful scrutiny.

We have attempted to produce these isotopes by ^{198}Pt(p,3pn)^{195}Os and ^{198}Pt(p,3p)^{196}Os reactions at 100 MeV and observe them by γ-ray spectroscopy using our He-jet recoil transport (HeJRT) facility. Based upon our reaction systematics (see Sect. 7.1.1), we anticipate cross sections of 100-200 μb and 25-50 μb for the (p,3pn) and (p,3p) reactions, respectively. The large quantities of all other neutron-deficient activities produced in the target and transported in the HeJRT system however, necessitates radiochemical separation of the Os

activities. In our first experiments, we attempted a continuous "on-line" separation of the Os fraction. The He stream was bubbled through a reaction flask containing a nitric acid solution at elevated temperatures. In this way, the transported recoil product nuclei were collected and trapped in the reaction flask, while the Os activities were distilled off as osmium tetraoxide. The radioactive OsO_4 was then collected in a sodium hydroxide receiver which was observed with a Ge(Li) spectrometer. Although copious quantities of activities from the Pt target (including ^{193}Os) were observed in the reaction flask, no activity was ever detected in the Os receiver. This lack of success was probably due to our attempt to perform the distillation by a continuous carrier-free separation. We plan to continue this work by doing the separation in a "batch" process whereby the activities will be collected for some length of time and then, following addition of carrier, the distillation will be performed. This type of batch process can then be successively repeated. If this is successful, the next step will be development of a procedure for milking Ir daughter activities from the Os fraction in this experimental arrangement. With these efforts, we hope to first observe and identify ^{195}Os and ^{196}Os and then, on completion of the tape-drive and timing mechanism for the HeJRT system (see Sect. V.B.) accurately characterize their decay properties.

(R. Collé, P. Gallagher and W. B. Walters)

D. Systematics of (x,x2p) Reactions for Production of Nuclei 'Two Protons Removed from Stability'

There are well over a dozen cases of unknown neutron-rich nuclei 'two protons removed from stability' which have not as yet been observed. These range from the light mass (below and up to the Fe-Ni-Zn) region to the rare-earth and heavy metal (W-Os-Pt) regions. In recent years, considerable effort by a number of laboratories has been made to reach these nuclei by (p,3p) reactions with high energy ($\tilde{\geq}$100 MeV) proton beams. These efforts have lead to the discovery of ^{184}Hf [T. E. Ward, Y. Y. Chu and J. B. Cumming, Phys. Rev. C8 (1973) 340], ^{236}Th [C. J. Orth, W. R. Daniels and B. J. Dropesky, Phys. Rev. C8 (1973) 2364], and ^{206}Hg [G. K. Wolf, Nucl. Phys. A116 (1968) 387], as well as intense searches [University of Maryland Nuclear Chemistry Progress Report MNC-4028-0012, p. 51 (1973)] for the still undiscovered ^{62}Fe, ^{190}W and ^{196}Os. Although proton induced reactions are usually employed, these neutron-rich nuclei can also be produced by high energy photonuclear and "fast" neutron-induced reactions, e.g., (γ,2p) and (n,n'2p) reactions. Unfortunately, a difficulty underlying the searches by any of these production methods is the scarcity of cross section or production yield data. The manifestation of the problem is that one cannot unequivocally discern whether the failure to detect a given product is due to a small production yield or to its short (but unknown) half-life. For this reason, without some reasonable estimate of the former, one can neither establish limits on the half-life nor even perceive

the necessity for redesigning the experiment. In an effort to obviate this situation we have undertaken a systematic study of these (x,x2p) reactions for incident protons, bremsstrahlung and fast neutrons on target nuclei with known 'two protons removed' products.

Radiochemically determined cross sections or integral atom yields have been obtained over a wide range of target masses. The systematics of the cross sections or yields as a function of the target mass and their distributions as a function of x (number of neutrons removed) for the 'two-protons removed' isotopes were studied. In most cases, odd-A monoisotipic nuclei were selected (for the obvious reasons) to obtain the x-distributions. In addition, several even-A targets were also used for the (x,x2p) reaction systematics. Except in the light mass ($A \leq 50$) region, radiochemical separations of the 'two protons removed' fractions were necessary because of the very low yields for their neutron-rich products with respect to the activities (especially neutron-deficient) from all the other isotopic fractions.

1. Proton-Induced Reactions at 100 MeV

The (p,3pxn) reaction cross sections at 100 MeV as a function of x for the four targets (^{51}V, ^{75}As, ^{133}Cs and ^{181}Ta) which have been measured are shown in Fig. 27. For comparison, the data for ^{238}U, taken from Ward et al., are also provided. In all cases, attempt was made to measure either directly or to extract appropriately total independent formation cross sections for each product. This was often achieved because the product

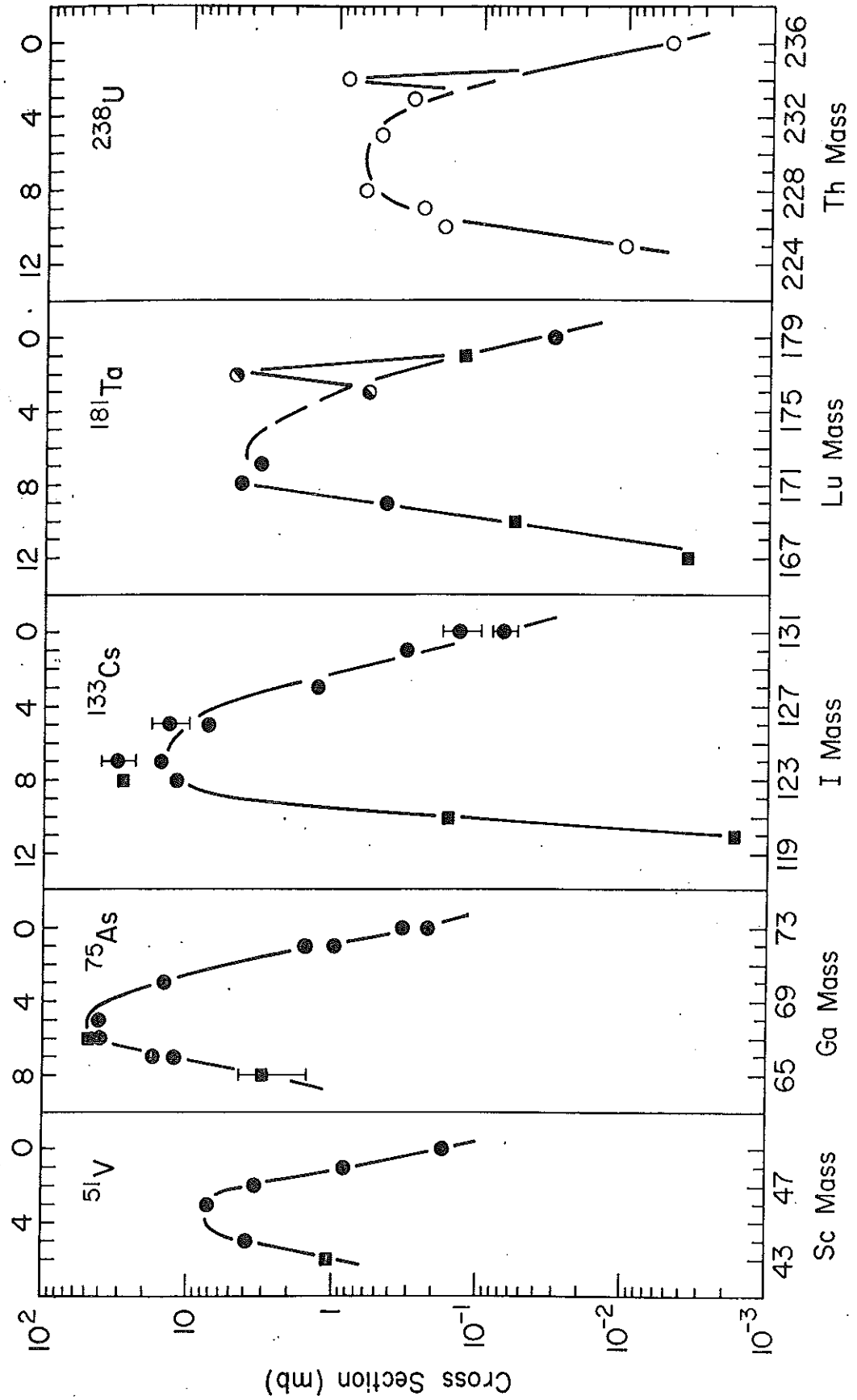

Fig. 27. Cross sections for (p,3pxn) reactions at 100 MeV.

activities were shielded by stable or long-lived isobars from decay through the mass chain. In other cases, by a judicious choice of irradiation, decay and counting time intervals the decay through the mass chain or isomeric states could be independently measured to make the appropriate corrections. These total independent formation cross sections are represented in the figure as closed circles. Especially for the very neutron-deficient products, this was not always possible and cumulative (from decay through the mass chain) formation cross sections were obtained. These are represented by the closed squares. The half-closed circles for ^{176}Ta and ^{177}Ta indicate that the cross sections are not the total for the product, but are only that for formation of one or more of its isomers. From these results two general trends are apparent. The cross sections for the entire distributions decrease with increasing mass of the target; and the distributions become steeper and narrower with lighter mass targets. The spike in the distribution at x = 2 for ^{238}U and possibly for ^{181}Ta may be ascribed to a strong contribution from a direct (p,p'α) knockout process. (we'll see this later)

The (p,3p) reaction cross sections at 100 MeV which have been measured are tabulated in Table 15 and have been plotted as a function of target mass in Fig. 28. The figure also contains the previous results of Ward et al. [D. L. Morrison and A. A. Caretto, Jr., Phys. Rev. 127 (1962) 1731; T. Ward, private communication, 1973-74]. As indicated, the cross section drops off rather rapidly with increasing target

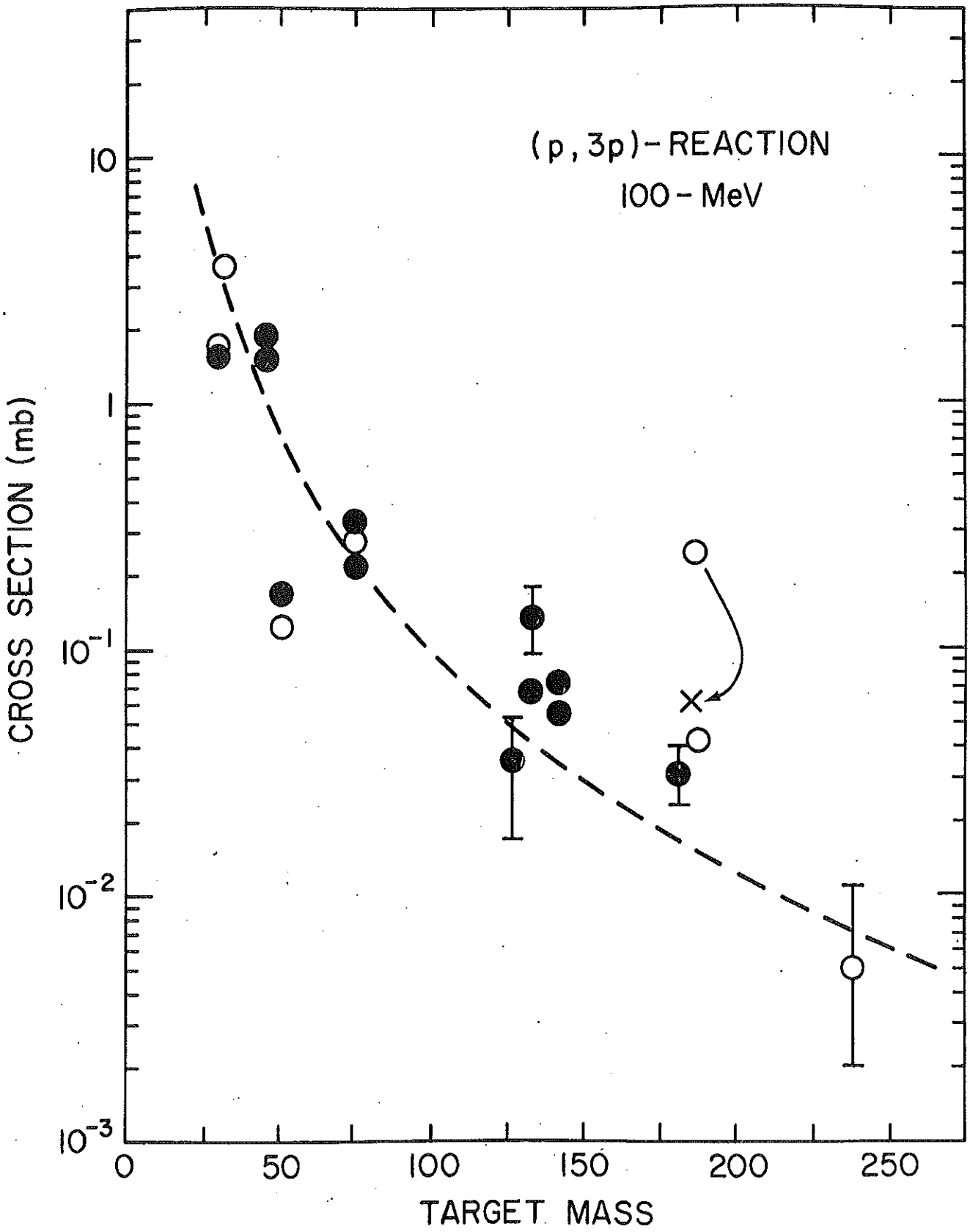

Fig. 28. The (p,3p) cross sections as a function of target mass.

mass. The dashed curve which reasonably simulates the rapid decrease in cross section was drawn with a cross section dependence proportional to A^{-3}. This functional dependence has no theoretical significance and is only meant to provide a basis for the magnitude of the dropoff.

An important trend of practical value in searching for unknown (p,3p) reaction products is that the ratio of the (p,3p) to (p,3pn) reaction cross section is nearly independent of target mass (see Table 15). This has the significance of allowing one to predict quite accurately the magnitude of the (p,3p) reaction cross section once the (p,3pn) reaction product is observed.

We intend to continue these systematics by undertaking another similar survey at a lower energy (e.g., 50-65 MeV). The (p,3p) reaction excitation functions in the region 100 to 400 MeV are known to gradually increase with energy. At higher energies, however, greater quantities of neutron-deficient products will be produced and the relative distributions of the neutron-deficient vs. neutron-rich products are often of more consequence than the absolute cross section values. Furthermore, the ^{69}Ga(p,3p) reaction excitation function has been shown [N. T. Porile, Phys. Rev. 125 (1962) 1379; N. T. Porile, S. Tanaka, H. Amano, M. Furukawa, S. Iwata and M. Yagi, Nucl. Phys. 43 (1963) 500] to have a strong energy dependence only to about 50 MeV. For these reasons, it would be of great interest to ascertain if a more favorable distribution of products at lower energies shifted to the neutron-rich side would compensate for the lowered cross sections.

Table 15

TARGET	PROTON-INDUCED (1) $\sigma[p,3p]$ (mb)	PROTON-INDUCED (1) $\frac{\sigma[p,3p]}{\sigma[p,3pn]}$	PHOTONUCLEAR (2) $Y[\gamma,2p]$	PHOTONUCLEAR (2) $\frac{Y[\gamma,2p]}{Y[\gamma,2pn]}$	NEUTRON-INDUCED (3) $Y[n,n2p]$	NEUTRON-INDUCED (3) $\frac{Y[n,n2p]}{Y[n,2n2p]}$	NEUTRON-INDUCED (3) $\frac{Y[n,2p]}{Y[n,n2p]}$
^{30}Si	1.58 ± 0.16	—	$2.54(10^{-3})$	—	$4.17(10^{-1})$	—	—
^{45}Sc	1.50 ± 0.51	0.201	$2.18(10^{-3})$	0.494	$1.41(10^{-1})$	0.342	0.204
	1.90 ± 0.21	0.199					
^{51}V	0.170 ± 0.016	0.195	$6.25(10^{-4})$	0.464	$7.27(10^{-2})$	0.387	—
^{75}As	0.219 ± 0.035	0.222	$5.67(10^{-5})$	0.474	$8.03(10^{-2})$	0.343	0.148
	0.328 ± 0.050	0.209	$1.65(10^{-4})$	0.469			
^{127}I	0.035 ± 0.018	0.212	$1.39(10^{-5})$	0.437	$4.24(10^{-2})$	0.219	—
^{133}Cs	0.068 ± 0.013	0.218	$4.90(10^{-6})$	0.410	$3.84(10^{-2})$	0.297	0.022
	0.137 ± 0.042	0.217					
^{142}Ce	0.072 ± 0.019	—	$9.09(10^{-6})$	—	$5.31(10^{-2})$	—	—
	0.054 ± 0.014	—					
^{181}Ta	0.0305 ± 0.0075	0.239	$1.92(10^{-6})$	0.391	$3.46(10^{-2})$	0.323	—
^{238}U*	0.005 $\pm$ 0.006 $\pm$ 0.003	(0.25)	—	—	—	—	—

(1) 100 MeV proton induced cross sections and cross section ratios. *Results for ^{238}U were taken from Orth, et al, Phys. Rev. C8 (1973) 2364.

(2) ≈ 90 MeV bremsstrahlung-induced photonuclear yields relative to $^{197}Au(\gamma,n)^{196}Au$ and yield ratios.
$Y = \int_{E_{TH}}^{90} \phi(E)\ \sigma(E)\ dE \ / \ \int_{8}^{90} \phi(E)\ \sigma_{Au}(e)\ dE.$

(3) "Fast" neutron-induced yields relative to $^{12}C(n,2n)^{11}C$ and yield ratios.
$Y = \int_{E_{TH}}^{E_{MAX}} \phi(E)\ \sigma(E)\ dE \ / \ \int_{20.2}^{E_{MAX}} \phi(E)\ \sigma_{C}(E)\ dE.$ Neutron spectrum from 100 MeV protons on ≈ 2.2 " Al stop.
Yields for (n,n^2p) and (n,2n2p) include contributions from $(n,^3He)$ and (n,α), respectively.

We also plan to compare our experimentally determined cross sections to calculations based on a Monte Carlo intranuclear cascade-statistical evaporation model [I. Dostrovsky, Z. Fraenkel and G. Friedlander, Phys. Rev. 116, 683 (1959); N. Metropolis, R. Bivins, M. Storm, A. Turkevich, J. M. Miller and G. Friedlander, Phys. Rev. 110, 185, 204 (1958); K. Chen, Z. Fraenkel, G. Friedlander, J. R. Grover, J. M. Miller and Y. Shimamoto, Phys. Rev. 166, 949 (1968); K. Chen, G. Friedlander and J. M. Miller, Phys. Rev. 176, 1208 (1968); K. Chen, G. Friedlander, D. Harp and J. M. Miller, Phys. Rev. C4, 2234 (1971)] using the VEGAS code of Chen, et al. for the cascade stage and the DFF code of Dostrovsky, Fraenkel and Friedlander for the evaporation stage.

(R. Collé and W. B. Walters)

2. Photonuclear Reactions with 90 MeV Bremsstrahlung

A survey of (γ,2pxn) reactions with 90 MeV bremsstrahlung, similar to that for the (p,3pxn) reaction systematics, was performed utilizing the National Bureau of Standards Electron LINAC. An approximate five-step 90-MeV bremsstrahlung distribution for this facility was determined radiochemically using five threshold monitor reactions which have known (assumed) excitation functions. For each reaction, an "effective" cross section obtained from a numerical integration of the excitation function (see inset Fig. 29) was used to obtain the "effective" number of photons from the reaction threshold to the maximum photon energy. A five-step spectrum of bremsstrahlung photons was then obtained by taking differences. This first distribution

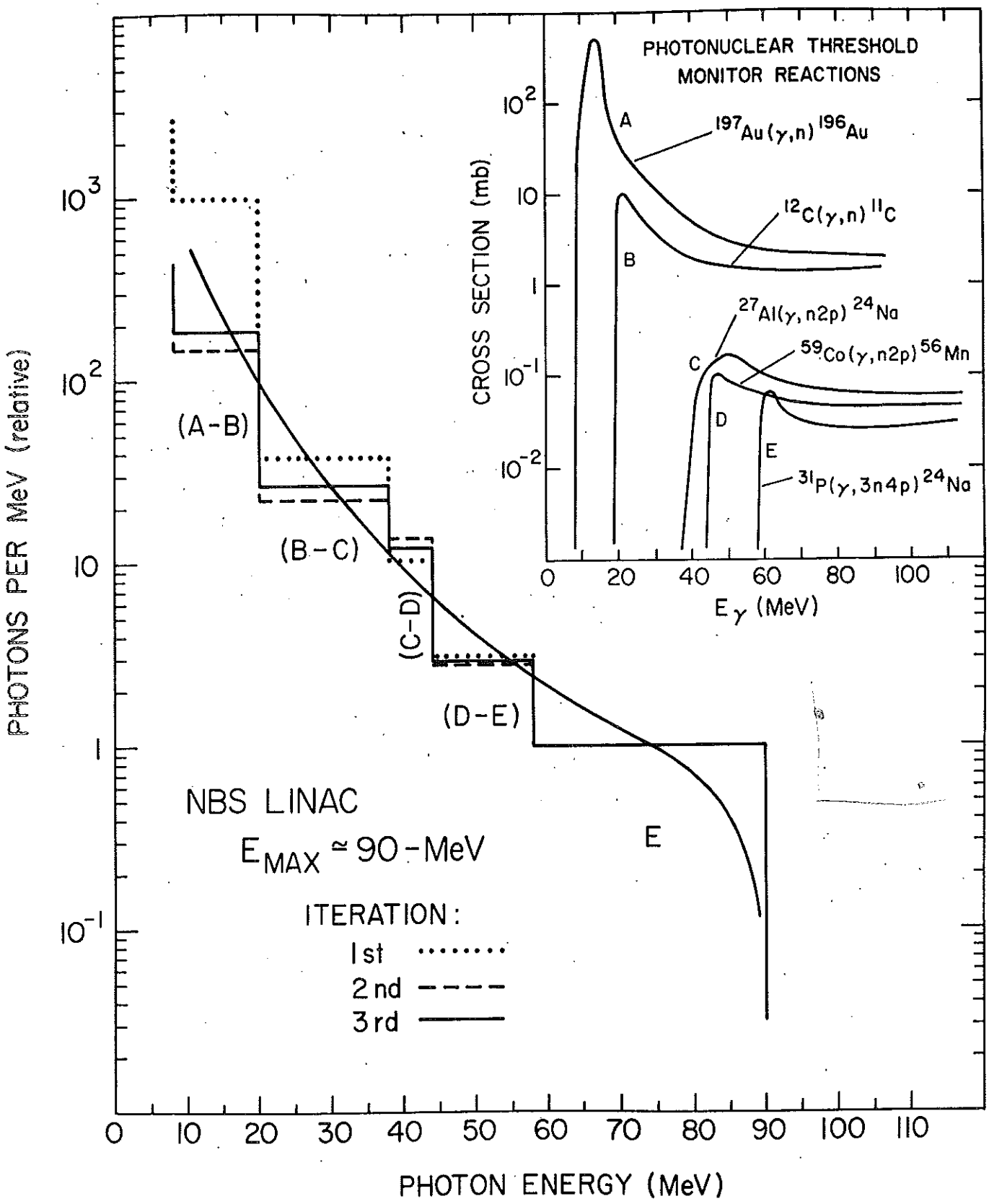

Fig. 29. Bremsstrahlung Distribution for 90 MeV Electrons.

was then folded back into the excitation functions and on numerically integrating, used to obtain new "effective" cross sections which were in turn used to obtain a new photon spectrum. This iterative procedure was then successively repeated until the refinements converged (i.e., when the changes in the spectrum became very small). The bremsstrahlung distribution obtained after three such iterative successive approximations is shown in Fig. 29. In Fig. 30, this approximate experimental result is compared to Monte Carlo electron-photon cascade calculations [M. J. Berger and S. M. Seltzer, Phys. Rev. C2, 621 (1970)] for 30- and 60-MeV bremsstrahlung spectra.

Integral atom yields for (γ,2pxn) reactions relative to the $^{197}Au(\gamma,n)$ monitor reaction for four targets as a function of x are provided in Fig. 31. The yields are given by

$$Y = \int_{E_{th}}^{E_{max}} \phi(E)\ \sigma(E)\ dE$$

where $\phi(E)$ is the bremsstrahlung flux distribution (photon spectrum) and $\sigma(E)$ is the cross section. Similar to that of Fig. 27, the closed circles and squares correspond, respectively, to total independent yields and cumulative yields. The trends in the product distributions are similar to those for the (p,3pxn) reactions. A direct comparison with Fig. 27 however indicates that the distributions decrease much more rapidly with increasing target mass, and their distributions are, in general, steeper. In addition, the peaks of the distributions

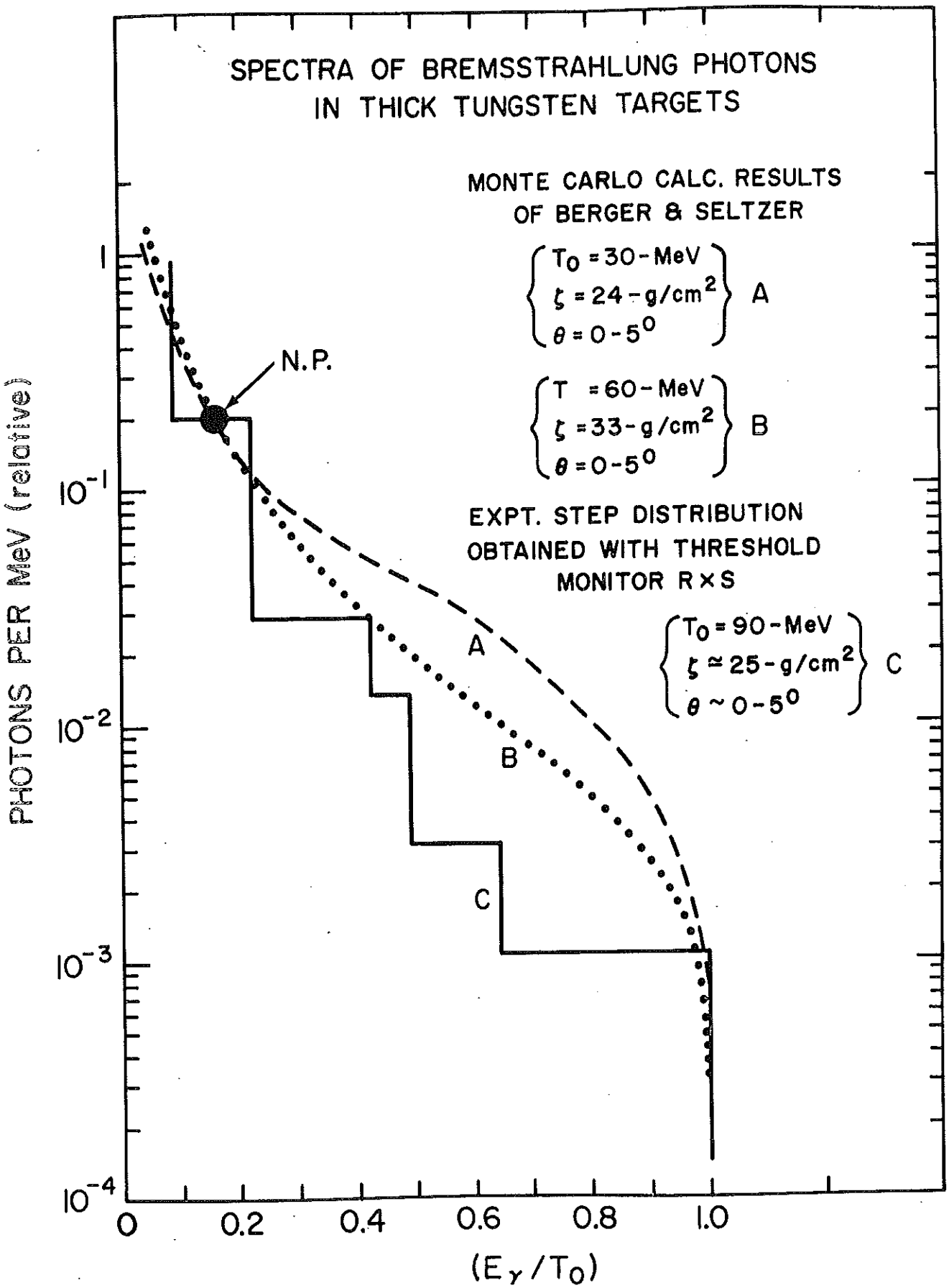

Fig. 30. Bremsstrahlung spectra in thick targets.

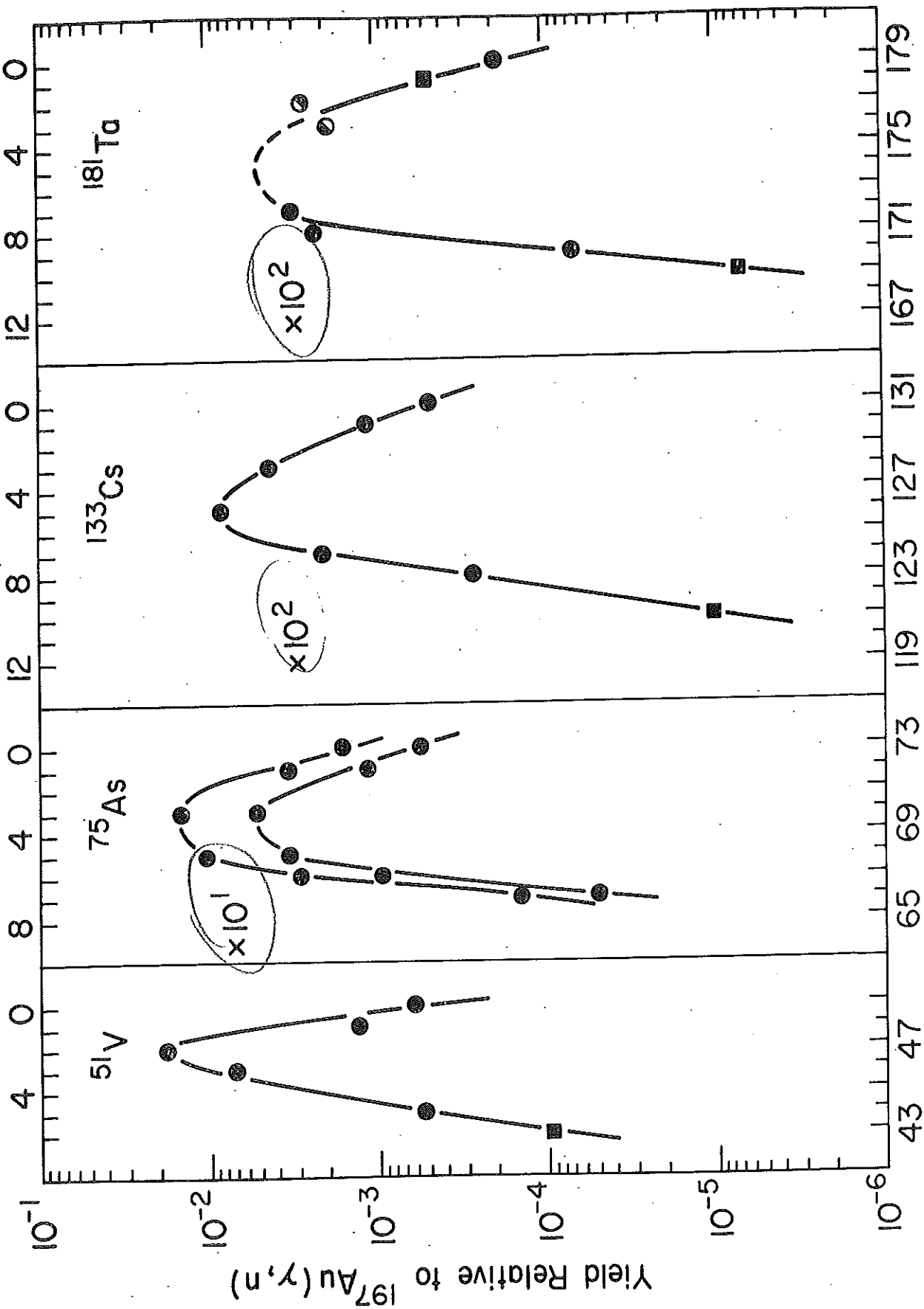

Fig. 31. Relative yields for the $(\gamma,2pxn)$ reaction with 90 MeV bremsstrahlung.

are shifted to more neutron-rich nuclei. The rapid decrease in yield with increasing target mass is illustrated in Fig. 32 for the (γ,2p) reaction. The three dashed curves in the figure have a functional dependence of A^{-3}, A^{-4} and A^{-5}. As indicated most of the data lie between the lower two curves. This can be contrasted to the (p,3p) reaction cross sections (Fig. 28) which were reasonably represented by the A^{-3} curve. Although the yields decrease much more rapidly with increasing mass, the ratios of (γ,2p) to (γ,2pn) reaction yields (see Table 15, column 4) are also nearly independent of target mass. As with proton-induced reactions, this is of great value in searching for unknown 'two protons removed' products.

These studies and their comparison to the proton-induced reactions are continuing. In addition to similar surveys at other energies we also plan to measure several complete excitation functions for the (γ,2p) and (γ,2pxn) reactions. Comparison of the present results at 90 MeV with some previous work on ^{51}V [M. Weisfield, Ph.D. Thesis, Rensselaer Polytechnic Institute, 1970], ^{75}As [T. T. Sugihara and I. Halpern, Phys. Rev. 101 (1956)], and ^{133}Cs [T. Kato and H. T. Tsai, J. Inorg. and Nucl. Chem. 36 (1974)] at both lower and higher energies suggest that lower energies would be preferable for production of neutron-rich nuclei. Although the yields increase with energy, the distribution of neutron-deficient with respect to neutron-rich products become much less favorable. At the present time however, the steepness of the distributions appear to make the photonuclear production method less favorable than

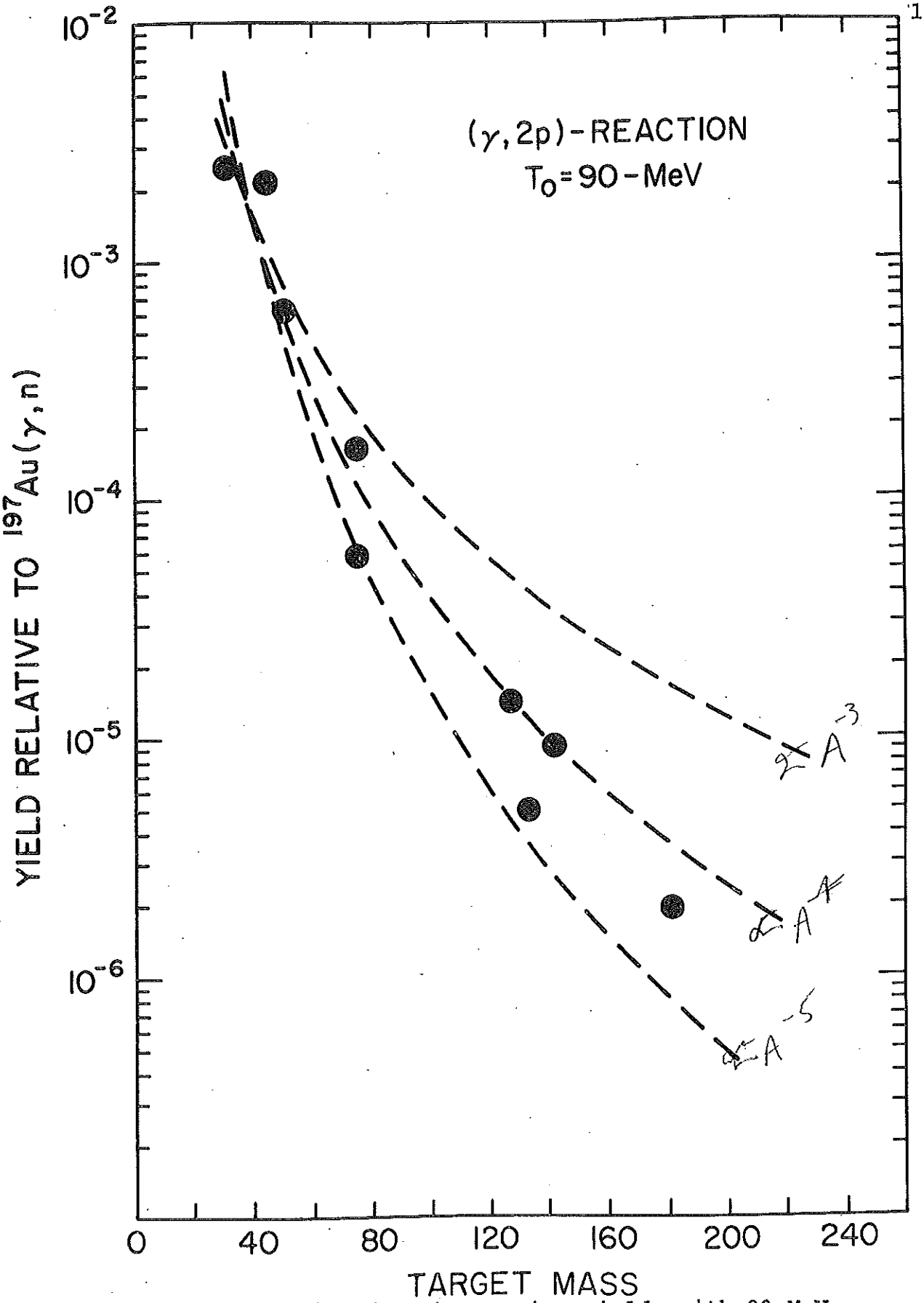

Fig. 32. Relative (γ,2p) reaction yields with 90 MeV bremsstrahlung as a function of target mass.

that by proton-induced reactions, except possibly in special cases, e.g., light mass region.

(R. Collé, W. B. Walters, W. H. Zoller and W. R. Dodge)

3. "Fast" Neutron-Induced Reactions

We have utilized the "fast" neutron spectrum accompanying the stopping of 100 MeV proton beams in a ~2.2" Al beam stop to investigate the (n,2pxn) reactions. The $^{12}C(n,2n)^{11}C$ monitor reaction (threshold ≃ 20.2 MeV) was used to estimate the "fast" neutron flux from this facility. Assuming an "effective" cross section of 9.5 mb, a flux of neutrons of ~4-5 x 10^9 n/cm^2 per μA of protons was obtained. This flux is only that for neutrons of energy greater than 20.2 MeV. Integral atom yields for several reactions leading to neutron-rich products obtained with this neutron spectrum are given in Fig. 33. The yields relative to the $^{12}C(n,2n)^{11}C$ monitor reaction are plotted as a function of target mass. Similar results obtained by T. Ward with a neutron spectrum from 200 MeV protons on an 18" water stop are also provided (open circles) in the figure. As indicated, the [(n,^{3}He)+(n,n2p)] reaction yields do not decrease as rapidly with increasing mass as the corresponding (p,3p) and (γ,2p) reactions do. For comparison to the proton-induced and photonuclear reactions, the A^{-3} curve (dashed) is also shown in the figure. The ratio of the (n,n2p) to (n,2n2p) reaction yields, again appear to be nearly constant (see Table 15, column 5) as the corresponding proton-induced and photonuclear reactions. Although the (n,2p) reaction yields

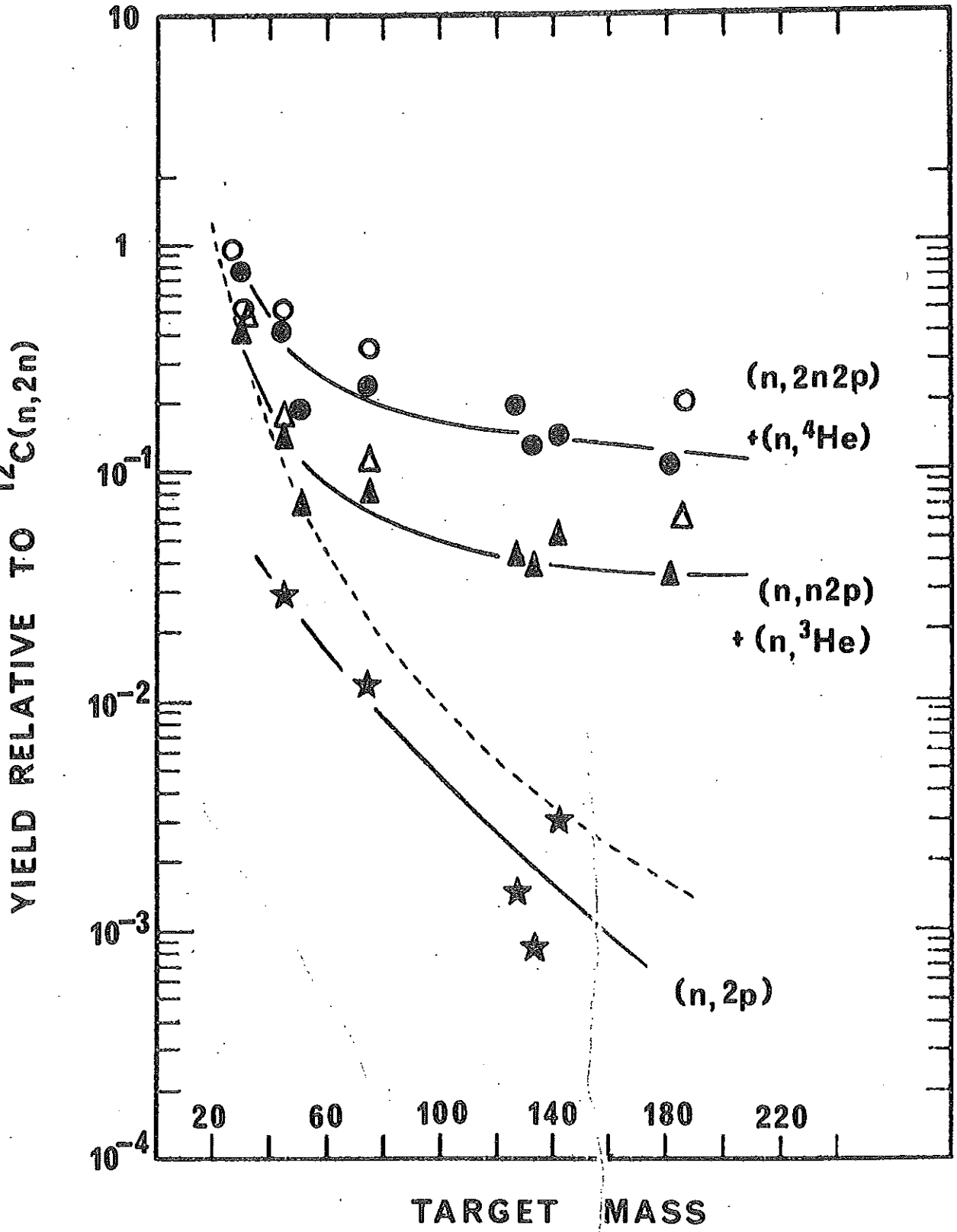

Fig. 33. Integral atom yields for fast-neutron induced reactions as a function of target mass.

are relatively low, these reactions are of special consequence. These reactions could open an entire new region of investigation since their products are one neutron-richer than the 'two protons removed from stability' products and their number which are presently unknown is legion. Although this production method is clearly more favorable for the medium and heavy mass region than the proton-induced or photonuclear reactions, unless the "fast" neutron flux is increased by at least a factor of 100, it would be difficult to pursue this production mechanism for producing new neutron-rich products.

(R. Collé and W. B. Walters)

4. Production of ^{43}K

As a result of the possible importance of 22.2 hr ^{43}K as a radionuclide imaging agent for diagnostic myocardial scanning, we have continued [University of Maryland Nuclear Chemistry Progress Report MNC-4028-0012, p. 85 (1973)] measurements of its production cross sections from Sc and Ca targets with high energy protons.

The following cross sections for production of ^{43}K and its major contaminant ^{42}K (12.36 hr) from Sc and Ca targets (natural isotopic abundances) with 100 MeV protons were obtained:

$^{45}Sc(p,3p)^{43}K$	1.90±0.21 mb/Sc atom 1.50±0.51
$^{45}Sc(p,3pn)^{42}K$	9.54±1.43 7.46±1.88
$Ca(p,2pxn)^{43}K$	0.335±0.040 mb/Ca atom
$Ca(p,2pxn)^{42}K$	0.607±0.067

Although the ^{43}K production cross section from Sc targets is greater than that from Ca, this is mainly a result of the low isotopic abundance of the neutron-rich Ca isotopes [^{44}Ca (2.08%); ^{46}Ca (0.003%); ^{48}Ca (0.19%)] which are the only ones contributing to the ^{43}K yield. The use of ^{44}Ca enriched targets would undoubtedly increase the ^{43}K yield, but it would not simply increase in proportion to the ^{44}Ca enrichment since a substantial contribution to the yield is from ^{48}Ca. Nevertheless, assuming that the ^{43}K is entirely produced from ^{44}Ca,

the $^{44}Ca(p,2p)$ cross section would be 16.1 ± 1.9 mb/^{44}Ca atom which is considerably greater than the $^{45}Sc(p,3p)$ cross section. Furthermore, the much larger quantities of contaminant activities from the Sc targets makes the use of Ca targets preferable. A summary of the yields (expressed as the activity produced per amount of target material and beam intensity) of ^{43}K and contaminant activities from Sc and Ca targets (nat. abun.) is provided in Table 16 for both saturation and a 12 hr irradiation. On inspection, it is apparent that with the Sc target all of the contaminant yields are greater. Moreso, for any reasonable decay period, many of the contaminant yields will still be over an order of magnitude greater than that for ^{43}K. For Ca targets in contradistinction, after a decay period of 8 hrs, all of the contaminants (except ^{42}K) are nearly an order of magnitude less than the ^{43}K yield. Although only the ^{42}K contaminant will remain following chemical separation of the target, the total activity for a thick Sc production target could exceed 3-Ci which would make handling the irradiated targets extremely difficult. Lastly, the ratio of ^{43}K to ^{42}K yields is at least a factor of 2-3 times more favorable with Ca targets. We therefore conclude that the best, but more costly in terms of target expense, method of production is from isotopically enriched (in ^{44}Ca and ^{48}Ca) Ca targets. We estimate that with an incident 100 MeV proton beam of 1 μA degraded to ≃50 MeV on passing through a 5 gm/cm^2 enriched (75-98% ^{44}Ca or 15-40% ^{48}Ca, at an estimated cost of $2000 per gram) CaO target, approximately 25-50 mCi of ^{43}K can be obtained in a 12 hr irradiation.

(R. Colle and W. B. Walters)

Table 16. Production of ^{43}K and contaminant activities from Sc and Ca (Natural Abundance) targets with 100 MeV protons.

	Half-Life (hr)	YIELD FROM Sc mCi/(g/cm^{2}Sc)(μA)		YIELD FROM Ca mCi/(g/cm^{2}Ca)(μA)	
		Saturation	12-hr Irrad.	Saturation	12-hr Irrad.
^{43}K	22.2	4.29	1.34	0.849	0.265
^{42}K	12.36	21.6	10.6	1.54	0.753
^{48}Sc	43.7	--	--	0.0395	0.00685
^{47}Sc	81.84	--	--	0.149	0.0144
^{44m}Sc	58.6	220 - 320	30 - 45	0.0631	0.00835
^{44g}Sc	3.93	110 - 220	95 - 190	0.188	0.165
^{43}Sc	3.89	220 - 440	190 - 380	0.192	0.169
^{47}Ca	108.96	-	-	0.373	0.0274
^{45}Ti	3.078	8.6 - 17.	8 - 16	--	--
^{41}Ar	1.83	2.1	2.1	0.139	0.137

B. He-Jet System Sections

1. He-Jet Recoil Transport System

A He-jet recoil transport (HeJRT) system is being built in pursuance of our interest in studying short-lived radioactive products in both very neutron-excess and -deficient regions (cf. Sections IIG and IIK). The essentials of this technique have been previously described [R. D. Macfarlane and R. D. Griffioen, Nucl. Instr. and Meth. 24, 461 (1963); R. D. Macfarlane, R. A. Gough, N. S. Oakey and D. F. Torgerson, Nucl. Instr. and Meth. 73, 285 (1969); H. Dautet, S. Gujrathi, W. J. Wiesehahn, J. M. D'Auria and B. D. Pate, Nucl. Instr. and Meth. 107, 49 (1973)]. Basically, radioactive product nuclei recoiling out of a target following a nuclear reaction are trapped into molecular clusters in a doped (e.g. with water vapor) He gas stream and transported to a remote collection-detection station by differential pumping. The radioactive products are then collected for study by either adsorption onto a stationary surface or onto a moving tape. Alternatively, the product nuclei could be collected into a solution for subsequent "on-line" or "batch" radiochemical separations [K. L. Kosanke, W. C. McHarris, R. A. Warner and W. H. Kelly, Nucl. Instr. and Meth. 115, 151 (1974)] by bubbling the He stream through a reaction flask. Then, depending upon the specific case in question, the collected radioactive nuclei are studied by detecting and assaying the decay γ rays, x rays, α-particles, etc.

In designing and constructing our system, we have tried to incorporate a great deal of flexibility in order to handle a wide variety of applications, and in the process have borrowed a

number of the most desirable design features from several existing systems, such as those at Yale, Texas A&M, Michigan State and Washington Universities. Following are brief descriptions of the various components of the HeJRT system and their present stage of development. To date, the system has been tested by transporting the activity onto stationary collectors and bubbling through aqueous solutions using pressure differentials of ~3 atm He to atmospheric pressure.

2. Gas Supply and Doping System

The 'bubbler' apparatus used to dope the He gas is shown in Fig. 38. At present, only water vapor as a doping agent for formation of molecular clusters is being used. Although others could be readily employed in the existing system, their use is not anticipated because of the proven sucess of He/H_2O mixtures. Helium from a supply tank in the cyclotron upper chemistry laboratory area after regulation and monitoring its flow rate with a manostat flow meter is admitted to a gas dispersion tube (bubbler) where the He is saturated with H_2O vapor. The H_2O-doped He gas stream then travels approximately 14 meters to the target chamber which is located on the end of the cyclotron beam line A.

3. Target Chamber Assembly

A schematic of the target chamber assembly is also shown in Fig. 38. The incident cyclotron beam before entering the target chamber passes through a 0.435-mil Havar vacuum foil which seals the target chamber from the beam line vacuum. The ~2.5-cm diam window assembly also serves as a collimating aperture for the target chamber. Two other vacuum foils (both 0.435-mil Havar) upstream from this window serve as precautionary devices to protect the cyclotron vacuum. The beam line sections

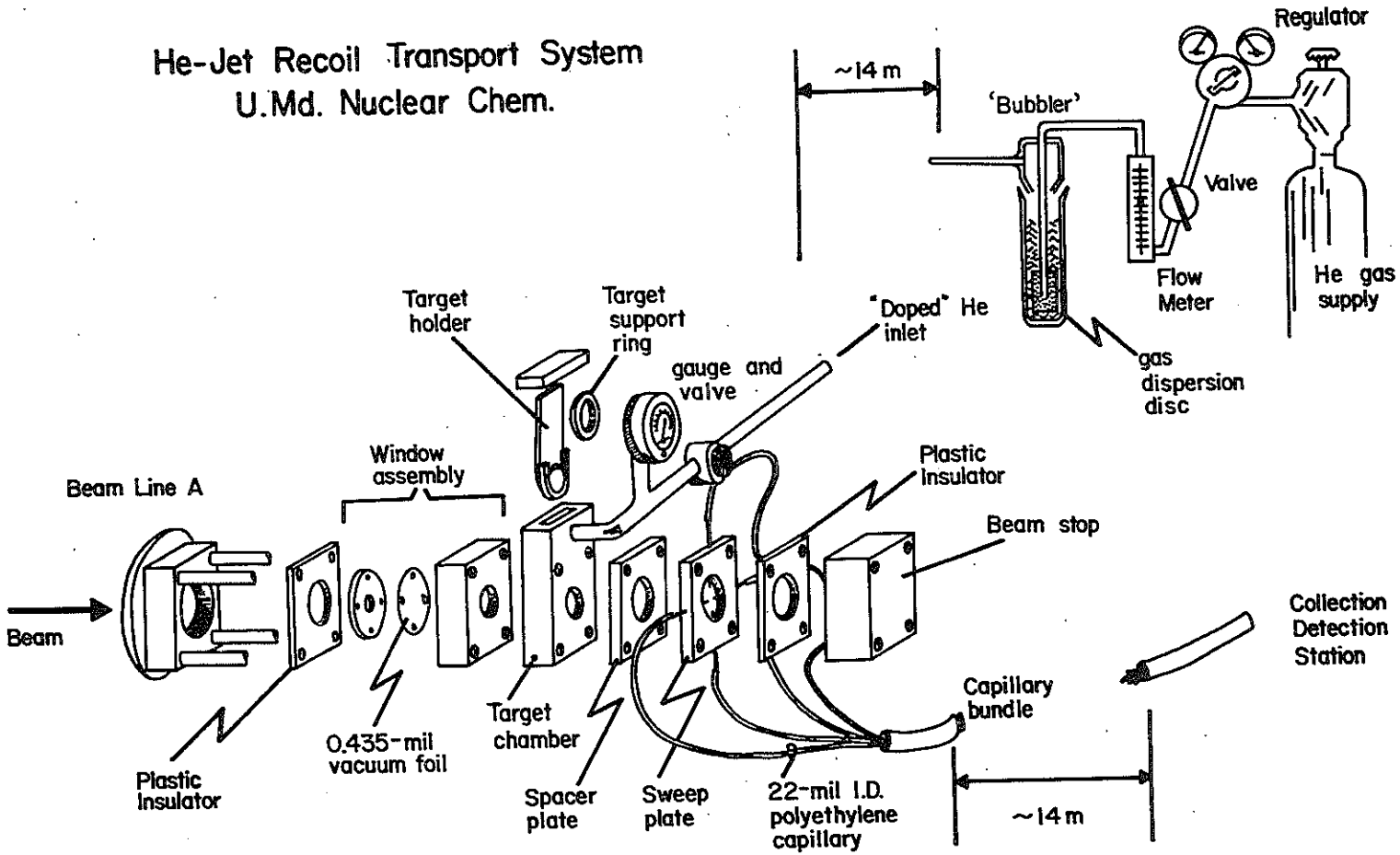

Fig. 38. Schematic drawing of He JRT system.

between these foils are independently evacuated. On entering the target chamber, the beam passes through a 2.5-cm diam target (which is held in place by a ring support in the target holder tongue) and then into the thermalization region, and finally stops in a high purity aluminum beam dump which also serves as a Faraday cup. The target chamber is electrically insulated from the beam line and beam stop with plastic insulators. The thermalization region consists of a variable thickness spacer plate (selected appropriately to adjust for the recoil range of the radioactive products) and a sweep plate. The radioactive products which recoil out of the target are thermalized in a He atmosphere of 1-3 atm saturated with water vapor and swept out through four 22-gauge stainless steel hypodermic needles in the sweep plate. The total internal volume of the target chamber (including thermalization region) defined by the window and beam stop is $\simeq$90-cm^3. A capillary bundle of four 22-mil ID polyethylene capillaries which are connected to the hypodermic needles transport the activity ~14 meter by differential pumping to the remote collection-detection station in the upper chemistry area.

4. Collection-Detection Station

Differential pumping for transporting the activity is accomplished by maintaining a large pressure difference between the target chamber and collection station. For "on-line" or "batch" chemical separation operations, this is achieved by maintaining the low pressure end at atmospheric pressure (or possibly at the vapor pressure of the solution into which the activity is transported) and the high pressure end at 3-4 atm.

Otherwise, the activity is transported to a low pressure collection chamber by differential pumping with a 3100 liter/min Kinney KDH-130 single-stage rotary water-colled mechanical vacuum pump. The 14.5- x 28- x 38-cm stainless steel collection chamber is now completed and the pump is operable. The tape drive mechanism which will be housed in the collection chamber is presently under construction. The mechanism, utilizing 7-in reels of standard ¼-in audio tape onto which the activity impinges, will move the tape from the collection to detection station in less than several tenths of a second. The detection station is located on an extended arm of the collection box. Thus, considerable flexibility in the choice and configuration of detectors for different types of experiments will be possible by the use of different extension arms. Furthermore, the electronic timing control for the tape drive mechanism will permit many possible modes of operation.

5. Electronic Timing Control

The timing control for the tape drive mechanism is still under design. Its major function is to generate four variable time intervals which will determine the length of time the source is deposited on tape, the tape movement and positioning of the source in front of one or more detectors, and their counting times. The time intervals are obtained with a variable oscillator which drives a bank of four 4-decade scalters. The scalers count for time intervals preselected with four 4-decade thumbwheel switches. Thus, the time intervals are determined by the combination of the oscillator frequency and the value of the thumbwheel switch. When each

scaler reaches its programmed count as preselected by the thumbwheel switch, a gate signal is activated which either starts or stops the motor in the tape drive. The first gate signal at time t_1 starts the tape movement and it continues until the motor is stopped with the second gate signal at time t_2. The third gate signal at time t_3 again starts the motor and is stopped at time t_4 with the fourth gate signal which also resets the scalers. This cycle is then continuously repeat d. For a typical operation then, the time interval (t_3-t_2) would determine the length of time the source is deposited on tape; the time interval (t_4-t_3) when the tape moves would determine the position the source is moved to in front of a detector; and, the interval (t_1-t_4) would determine the counting time length. The last interval (t_2-t_1) when the tape again moves would determine a new position for deposition of the source. Similarly, these time intervals could also be used to move the source to successive positions in front of two or more detectors. The timing gate signals will also be used to automatically start and stop analysis and storage of the counting data in the cyclotron IBM-360/44 computer data acquisition system. Obviously, considerable flexibility is possible because of these four independent preselectable timing intervals.

(R. Collé, P. Gallagher and W. B. Walters)

D. Upgrading of the Packard Analyzer System

We have completed our work at upgrading our older Packard Multichannel Analyzer System acquired in 1965-1967 which consists of a Model 45 10^6 count/channel memory, a Model 123 Buffer organizer-tape deck interface, a Potter 7-track tape deck, and a few other modules. We have upgraded the performance of the system by replacing the older 20 MHz 4096 ADC's by new Northern Scientific 100 MHz 8192 ADC's. It proved possible to directly interface the new ADC's into the older analyzer by changing connectors and adding 2 extra signal wires. As a result, the resolution and speed of analysis for the Packard system is now of similar quality to our newer systems.

(S. V. Jackson, W. H. Zoller, and W. B. Walters)

E. Cyclotron Chemistry Laboratory

During the past year, the hoods have been installed and connected both for ventillation and water in the upper chemistry area at the Cyclotron Laboratory. We are now able to chemically separate the nuclides we seek prior to removing the sources from the Cyclotron Laboratory.

(W. B. Walters, R. Colle, and P. Gallagher)

F. CLSQ: A Multicomponent Decay Curve Analysis Program

The Brookhaven multicomponent decay curve analysis program, CLSQ, has been adopted for use on the University of Maryland UNIVAC-1108 computer. Based on an iterative procedure for a least-squares fitting of the exponential decay functions, this program is widely used in many laboratories throughout the world and is generally recognized as one of the best. It has considerable flexibility in handling many different types of problems while still maintaining user simplicity. Its main features are:

(1) Can process sequentially an unlimited number of problems (subject to time limitations only).

(2) For each problem, the program can treat up to 200 data points with as many as 10 components. [Note: It can easily be modified to increase these limits, although this is probably meritless.]

(3) Has two input options depending on whether the count rates with uncertainties are input or whether these are to be calculated directly from the counting data.

(4) Makes gackground subtractions and calculates appropriate statistical uncertainties if called for.

(5) Makes counter dead-time corrections when known. This is only for fixed counter dead-times, e.g. for proportional counters, etc.

(6) Has provision for data rejection based on several optional criteria.

(7) Can make known component subtraction.

(8) Will fit known half-lives, unknown half-lives or combinations thereof to obtain count rates at end of bombardment (or any other preselected time).

(9) Has provision for genetic relations of parent-daughter pairs.

(10) Makes error analyses and provides uncertainties for all unknown half-lives and count rates at end of bombardment.

(11) Provides an estimate of the goodness-of-fit and indicates whether the fit was convergent.

The program including the mathematical method has been previously described [J. B. Cumming, National Academy of Sciences--National Research Council, Nuclear Science Series Rpt. NAS-NS-3107, p. 25 (1962]], and although it has undergone substantial revisions over the years, the method and input requirements remain similar.

(R. Collé)

G. CYMMA and CXEMA: Programs for Analysis of Decay Scheme Data

Two programs have been written to aid in analyzing, correlating and balancing observed γ-ray transitions for ellucidations of nuclear level and radioactive decay schemes. The first, CYMMA, attempts to detect cascade and crossover γ-ray transitions by making a sums-and-differences energy analysis of observed (input) γ-ray transitions. The second, CXEMA, attempts to place observed γ-ray transitions in known (input) level schemes by fitting (i.e., matching) the observed γ-ray energies to the known energy level differences. For both programs, the criterion for energy agreements (i.e., matches) is an input variable. The input requirements for both programs are similar, such that the majority of input data cards are compatible with both programs. The programs are quite simplistic and as a result of their inherent limited nature, extreme caution (with respect to any implied inclusiveness) must be exercised with their use. Nevertheless, they are suitable for a rapid first analysis when one is confronted with a copious quantity of observed transitions, and they have the redeeming significance of saving considerable time and effort over the more tedious manual bookkeeping procedures.

(R. Collé)